Fluid helicity and dynamo effect

N. Seehafer, A. Demircan, F. Feudel

Institut für Physik, Universität Potsdam, PF 601553, 14415 Potsdam, Germany

Abstract

Using the incompressible magnetohydrodynamic equations, we have numerically studied the dynamo effect in electrically conducting fluids. The necessary energy input into the system was modeled either by an explicit forcing term in the Navier-Stokes equation or fully selfconsistently by thermal convection in a fluid layer heated from below. If the fluid motion is capable of dynamo action, the dynamo effect appears in the form of a phase transition or bifurcation at some critical strength of the forcing. Both the dynamo bifurcation and subsequent bifurcations that occur when the strength of the forcing is further raised were studied, including the transition to chaotic states. Special attention was paid to the helicity of the flow as well as to the symmetries of the system and symmetry breaking in the bifurcations. The magnetic field tends to be accumulated in special regions of the flow, notably in the vicinity of stagnation points or near the boundaries of convection cells.

Key words:
Magnetohydrodynamics, convection, dynamo
PACS: 47.65.+a, 47.20.Bp, 47.20.Ky, 95.30.Qd

1 Introduction

Electrically conducting fluids in motion can act as self-excited dynamos. The magnetic fields of celestial bodies like the Earth and the Sun are generated by such dynamos. Their theory aims at modeling and understanding both the kinematic and dynamic aspects of the underlying processes. Realistic models, describing the dynamo processes, are given in the form of a complex system of nonlinear partial differential equations including the Navier-Stokes equation (NSE), the induction equation, the heat equation, and the thermodynamic equation of state. Heating causes fluid motions which in turn, notably in the presence of rotation, induce magnetic fields. For comprehensive accounts of dynamo theory we refer to Refs. [1–3].

It is generally accepted that the nonlinear system of the incompressible magnetohydrodynamic (MHD) equations contains the basic elements of a dynamo. It consists of the coupled system of the NSE for the flow and the induction equation for the magnetic field in the form

$$\frac{\partial \mathbf{v}}{\partial t} + (\mathbf{v}\cdot\nabla)\mathbf{v} = R^{-1}\nabla^2\mathbf{v} - \nabla p - \frac{1}{2}\nabla\mathbf{B^2} + (\mathbf{B}\cdot\nabla)\mathbf{B} + \mathbf{f}, \tag{1}$$

$$\frac{\partial \mathbf{B}}{\partial t} + (\mathbf{v}\cdot\nabla)\mathbf{B} = R_m^{-1}\nabla^2\mathbf{B} + (\mathbf{B}\cdot\nabla)\mathbf{v}, \tag{2}$$

$$\nabla\cdot\mathbf{v} = \mathbf{0}, \quad \nabla\cdot\mathbf{B} = \mathbf{0}, \tag{3}$$

where $\mathbf{v}$, p and $\mathbf{B}$ denote fluid velocity, thermal pressure and magnetic field, R and R_m the kinetic and magnetic Reynolds number, respectively, and $\mathbf{f}$ is a yet unspecified body force. The third and fourth terms on the right-hand side of Eq. (1) constitute the Lorentz force. Equations (3) impose the incompressibility condition on the fluid and ensure the source-free property of the magnetic field. The body force $\mathbf{f}$ on the right-hand side of the NSE has to be specified in the concrete physical context and is the sum of all forces that drive the fluid, as e.g. the buoyancy force in thermal convection, or modify the motion, like the Coriolis force in a rotating star. It pumps energy into the fluid and we look for long lasting magnetic fields, not decaying as a result of the nonlinear coupling of NSE and induction equation. This phenomenon will be called nonlinear dynamo effect.

Traditional dynamo theory has been mainly kinematic, i.e., the induction equation, Eq. (2), is solved for a prescribed velocity field, disregarding the equation of motion, Eq. (1). In the kinematic frame the question is whether a fluid motion can amplify, or at least prevent from decaying, some weak seed magnetic field. Positive growth rates indicate instability of the zero magnetic field solution and we speak of a kinematic dynamo effect. A central result of traditional kinematic dynamo theory is that a nonvanishing kinetic helicity, for a given volume V defined by

$$H = \int_V \mathbf{v}\cdot(\nabla\times\mathbf{v})\,\mathrm{d}^3\mathbf{x}, \tag{4}$$

with $h = \mathbf{v}\cdot(\nabla\times\mathbf{v})$ being the helicity density, is favourable for a dynamo effect. An intensively studied example for helical dynamos are the ABC flows $\mathbf{v}_{\mathrm{ABC}}$ [4–6].

To take into account the back reaction of the magnetic field on the velocity field, the kinematic analysis has to be extended to studying the full nonlinear MHD equations, Eqs. (1)–(3). The velocity fields $\mathbf{v}_{\mathrm{ABC}}$ can be produced as steady solutions of the incompressible NSE, Eq. (1), if an external body force

$\mathbf{f}_{\rm ABC} = -\nabla^2 \mathbf{v}_{\rm ABC}$ is applied. In the first part of this paper we report bifurcation studies of the MHD equations with the forcing $\mathbf{f}_{\rm ABC}$ (detailed results are published in Refs. [7–12]; see also Ref. [13] where dynamo bifurcations in an array of driven convection-like rolls similar to the flow in the outer core of the Earth are studied). After that we present results on dynamo action in thermal convection. In this case, which corresponds to the situation in the Earth and in stars, the force driving the fluid motion is thermal buoyancy. It is not prescribed but selfconsistently obtained by solving the MHD equations coupled with a temperature equation.

2 Dynamo bifurcations in the ABC flows

2.1 Pure ABC forcing

One of the successful examples for producing a dynamo are the ABC flows (named after Arnold, Beltrami and Childress)

$$\mathbf{v}_{\rm ABC} = (A\sin k_0 z + C\cos k_0 y, B\sin k_0 x + A\cos k_0 z, C\sin k_0 y + B\cos k_0 x), \quad (5)$$

where A, B, C denote constant coefficients and k_0 is a wave number. They are strongly helical Beltrami flows. Beltrami flows are flows with parallel velocity and vorticity ($\nabla \times \mathbf{v}$) vectors. The ABC flows satisfy the Beltrami condition, $\nabla \times \mathbf{v} = \gamma \mathbf{v}$, with a constant γ, namely $\gamma = k_0$, which is a necessary condition for the existence of chaotic domains in Beltrami flows [4]. For this reason, they have received much interest [5,14], notably in the kinematic context as candidates for fast dynamos [6] (for which the growth rate remains bounded from below by a positive constant as the magnetic diffusivity tends to zero).

Imposing an external body force

$$\mathbf{f} = -\nabla^2 \mathbf{v}_{\rm ABC} = k_0^2 \mathbf{v}_{\rm ABC} \quad (6)$$

in the NSE and applying periodic boundary conditions with period 2π in all three spatial directions, Galanti et al. [15] investigated the system of the MHD equations [Eqs. (1)–(3)]. Numerically simulating the system for different Reynolds numbers and selected initial conditions, they observed that at some critical value of the Reynolds number the ABC flow with no magnetic field loses stability to a time-periodic state in which a magnetic field is excited and which, thus, represents a dynamo.

At this stage we started our study of the ABC dynamo, for the special case $A = B = C = 1$, $k_0 = 1$. The magnetic Prandtl number was set equal to unity, $P_m = R_m/R = 1$, so that the kinetic Reynolds number R was the only

remaining control parameter. R was raised from zero in small steps in order to detect bifurcations. For small R, there exists only one stable stationary solution, namely the ABC flow [given by Eq. (5)] with a vanishing magnetic field. Its symmetry group is the full equivariance group of the ABC forced MHD equations, the octahedral group O (the rotation group of the cube) [4,14,16].

For varying R, this steady-solution branch was traced and the Jacobian matrix and its eigenvalues were computed in each step. The table in Fig. 1 lists the solution branches detected, along with their regions of stability and symmetries. The numbers in the branch designations indicate the multiplicity of

Branch	Stability interval	Symmetry
ABC flow	$0<R<5.7$	O
Per–1	$5.7<R<11.5$	O
Per–3	$7.7<R<16.0$	D_4
Per–4	$11.5<R<17.3$	D_3
Torus–3	$16.0<R<20.0$	
Torus–4	$17.3<R<17.9$	
Chaos–3	$R\geq 20.0$	
Chaos–4	$R\geq 17.9$	

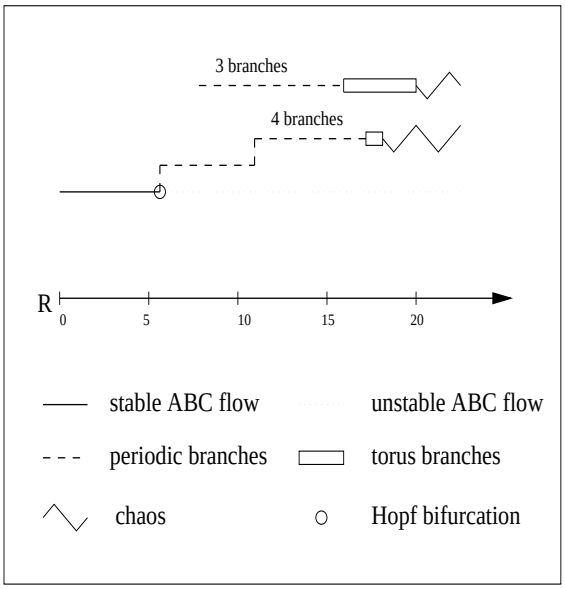

Fig. 1. Overview of the different solution branches (left). Schematic bifurcation diagram (right).

the branches, i.e. the number of coexisting conjugate branches. Per-3, for instance, stands for three coexisting branches of periodic solutions, each being invariant to one of three conjugate dihedral subgroups D_4 (D_4 is the group of all rotations and reflections which transform a square in a plane into itself). The primary ABC flow loses stability in a Hopf bifurcation in which a stable periodic branch with a nonvanishing magnetic field is born. Since only a single pair of complex-conjugate eigenvalues crosses the imaginary axis, the new branch, denoted as Per-1, retains the full symmetry O. More precisly, the solution is no longer point symmetric with respect to all symmetry transformations since some of these produce time shifts. However, the periodic orbit as a whole is invariant. In the right half of Fig. 1 a schematic bifurcation diagram is depicted. There are two main (stable) branches. One of them is generated by successive bifurcations from the primary ABC flow. The other one, appearing with Per-3, seems to be a result of a saddle-node bifurcation; its unstable counterpart has not been found.

Next we want to give an impression of the magnetic field structure in real (configuration) space. In kinematic dynamo studies using the ABC flow with $A = B = C$ cigar-like concentrations of the magnetic field about velocity stagnation points were observed [15,17]. The ABC flow with $A = B = C$ has eight stagnation points, which are unstable fixed points of the flow $\mathbf{v}$. The corresponding eigenvalues are real and have signs $(+,-,-)$ or $(-,+,+)$. The intersections of the stable and unstable manifolds of the stagnation points form a complicated web of heteroclinic lines [14]. Stagnation points with a two-dimensional stable manifold have been denoted as of α type and those with a two-dimensional unstable manifold as of β type. There are four stagnation points of each type. The cigar-like structures of the magnetic field observed for the kinematic problem are localized about the stagnation points of the α type. In Fig. 2 isosurfaces of the magnetic field strength are drawn. The cigar-like

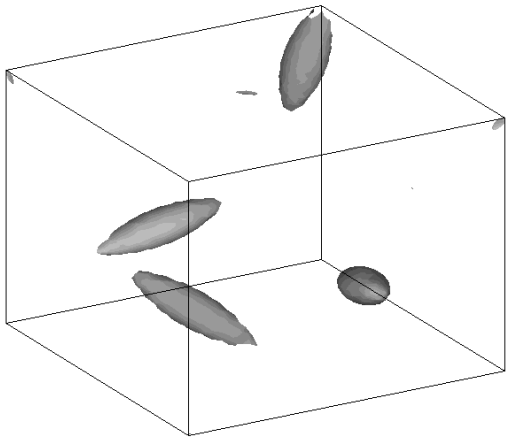

Fig. 2. Isosurfaces of the magnetic field with 65% of the maximal modulus for the symmetric branch at $R = 10$ (snapshot).

structures are clearly recognizable also in the nonlinear regime, where their shape now varies in time.

2.2 Generalized ABC forcing with varying helicity

In order to test the role of helicity for a dynamo effect we have, besides the pure ABC forcing given by Eqs. (5) and (6), also applied a generalized ABC forcing of the form

$$\mathbf{f} = (1-\lambda)\mathbf{v}_{\mathrm{ABC}} + \lambda \mathbf{v}^{-}_{\mathrm{ABC}}, \tag{7}$$

where we introduce

$$\mathbf{v}^{-}_{\mathrm{ABC}} = (A\cos k_0 z + C\sin k_0 y, B\cos k_0 x + A\sin k_0 z, C\cos k_0 y + B\sin k_0 x) \tag{8}$$

and λ is a parameter varying between 0 and 0.5 (but $A = B = C = k_0 = 1$ in all calculations described here). $\mathbf{v}^-_{\rm ABC}$ satisfies $\nabla \times \mathbf{v}^-_{\rm ABC} = -k_0 \mathbf{v}^-_{\rm ABC}$ and for a positive k_0 its helicity is thus negative whereas that of the original ABC flow is positive. The degree of helicity in the forcing varies with λ. For $\lambda = 0.5$ the addition of $\mathbf{v}^-_{\rm ABC}$ in the forcing term leads to a vanishing total helicity in the periodic box while $\lambda = 0$ corresponds to the original ABC forcing.

Fig. 3 gives a bifurcation diagram for the case of the generalized ABC forcing.

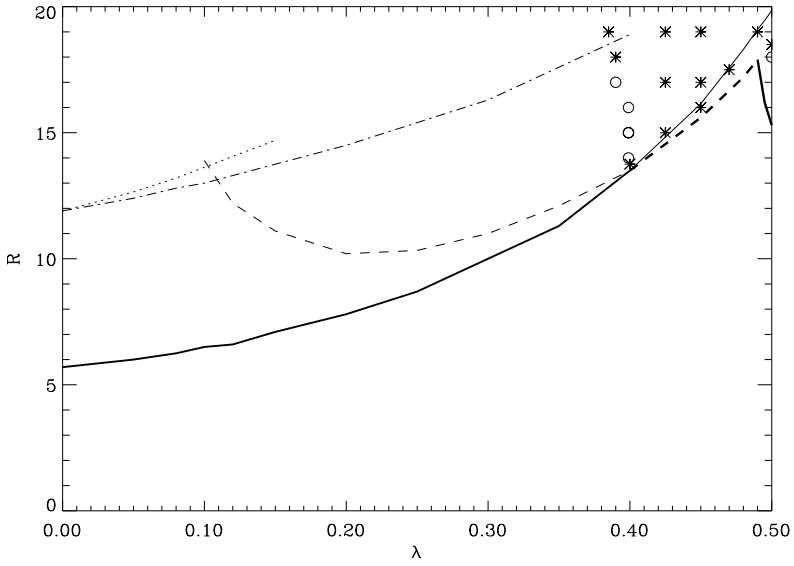

Fig. 3. Primary and secondary bifurcations of the original stationary solution in the λ-R plane. Solid line and dashed-dotted line: a single pair of complex conjugate eigenvalues crosses the imaginary axis; dashed line: two real eigenvalues pass through zero; dotted line: two pairs of complex conjugate eigenvalues cross the imaginary axis. Asterisks indicate points at which, by means of simulations, non-magnetic chaotic (Shilnikov-like) time-asymptotic states have been found, while circles correspond to magnetic periodic attractors.

For weak forcing (small R), there exists always a stable stationary, globally attracting solution (which coincides with the original ABC flow only in the special case of $\lambda = 0$). Keeping λ fixed and raising R, we have traced the steady-solution branch. For $\lambda < 0.4$ the steady state loses stability in a Hopf bifurcation, but at $\lambda = 0.4$ the type of the first bifurcation, as well as the character of the time-asymptotic states after this bifurcation, change. While for $\lambda < 0.4$ a magnetic periodic state is the (only) new attractor, for λ between 0.4 and 0.5 new *non-magnetic* states appear. The new non-magnetic stationary and periodic solutions bifurcating from the original stationary one for $0.4 < \lambda < 0.5$ are stable only over very small intervals of the bifurcation parameter R and lose their stability directly to non-magnetic chaotic states. The chaotic attractors found here are strongly suggestive of Shilnikov-type homoclinic chaos (for details see [7]).

3 Dynamo in asymmetric square convection

Studies of convection-driven dynamos have concentrated either on turbulent convection [18] or on convection near onset, where simple steady flows can be obtained [19,20]. For Rayleigh-Bénard Boussinesq convection with symmetric top and bottom boundary conditions, i.e. for convection with up-down reflection symmetry, the preferred convection pattern near onset is rolls. However, recent experimental and theoretical investigations show other possible attractors in this kind of convection. Resonant square and hexagon patterns appear in a range where only rolls were previously known to be stable [21–24]. Usually these *asymmetric* hexagons and squares, with rising or with descending motion in the center (and descending or rising motion near the boundary) are observed in convection lacking up-down reflection symmetry, namely in fluids with strongly temperature dependent viscosity or in Bénard-Marangoni convection [25–27], the asymmetric square pattern representing the dominating pattern over a wide range of the control parameters. Details about this pattern can be found in [23,24,28].

In this section we report on the dynamo properties of the asymmetric square pattern. We consider buoyancy-driven rotating convection in an electrically conducting plane fluid layer of thickness d heated from below. Using the Oberbeck-Boussinesq approximation, the governing system of partial differential equations now reads as follows:

$$\nabla \cdot \mathbf{v} = \nabla \cdot \mathbf{B} = 0 \tag{9}$$

$$\frac{\partial \mathbf{v}}{\partial t} + (\mathbf{v} \cdot \nabla)\mathbf{v} = -\nabla p + P \triangle \mathbf{v} + P R_a \, \theta \mathbf{e}_z + (\nabla \times \mathbf{B}) \times \mathbf{B} + P\sqrt{T}\, \mathbf{v} \times \mathbf{e} \tag{10}$$

$$\frac{\partial \mathbf{B}}{\partial t} + (\mathbf{v} \cdot \nabla)\mathbf{B} = P P_m^{-1} \triangle \mathbf{B} + (\mathbf{B} \cdot \nabla)\mathbf{v} \tag{11}$$

$$\frac{\partial \theta}{\partial t} + \mathbf{v} \cdot \nabla \theta = v_z + \triangle \theta \, . \tag{12}$$

Here p and θ represent the deviations of pressure and temperature from their values in the pure conduction state. We use Cartesian coordinates x, y and z with the z axis in the vertical direction parallel to the gravitational force. $\mathbf{e}_z$ is the unit vector in the vertical direction whereas the vector $\mathbf{e}$ is the general notation for the unit vector in the direction of the rotation axis. For our special choice $\mathbf{e} = \mathbf{e}_z$ one has $\mathbf{v} \times \mathbf{e} = (v_y, -v_x, 0)$ in Eq. (10). Equations (9)–(12) are given in usual dimensionless form. There are four dimensionless parameters, the Prandtl number P, the magnetic Prandtl number P_m, the

Rayleigh number R_a and the Taylor number T, defined by

$$P = \frac{\nu}{\kappa}, \qquad P_m = \frac{\nu}{\eta}, \qquad R_a = \frac{\alpha g d^3}{\nu\kappa}\delta T, \qquad T = \left(\frac{2\Omega d^2}{\nu}\right)^2, \tag{13}$$

where ν is the kinematic viscosity, κ the thermal diffusivity, η the magnetic diffusivity, α the volumetric expansion coefficient, g the gravitational acceleration, δT the temperature difference between lower and upper boundaries of the fluid layer and Ω the angular velocity of the rotation. The Rayleigh number R_a measures the strength of the buoyancy forces. We apply periodic boundary conditions with spatial period L in the horizontal directions x and y. The top and bottom planes are assumed to be stress-free, isothermal and impenetrable for matter and electromagnetic energy:

$$\frac{\partial v_x}{\partial z} = \frac{\partial v_y}{\partial z} = v_z = \theta = \frac{\partial B_x}{\partial z} = \frac{\partial B_y}{\partial z} = B_z = 0 \quad \text{at } z = 0, 1\,. \tag{14}$$

As in [29,30] we restrict ourselves to the case of a vanishing mean horizontal flow since such a flow can be removed by a Galilean transformation. L is kept fixed at a value of 4 and P at 6.8. The Taylor number, measuring the rotation rate, is restricted to values below the critical one for the Küppers-Lortz [31] instability. Here we find the primary convection patterns near onset to be never capable of dynamo action, neither with nor without rotation (for studies of dynamos in rapidly rotating plane layers see [32,33]). An example of steady up-square convection in the absence of rotation is shown in Fig. 4(a).

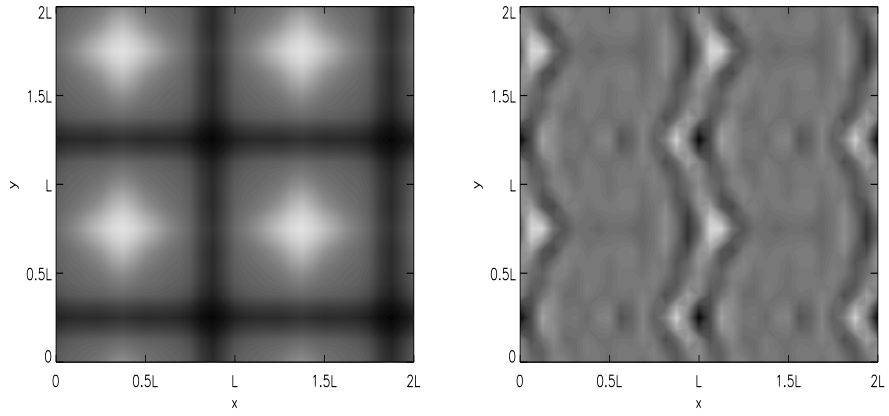

(a) (b)

Fig. 4. Shadowgraph images of the vertical velocity component v_z of an asymmetric square pattern for $R_a = 7000$ and $T = 0$ (a) and of the vertical component B_z of the associated unstable magnetic eigenmode for $P_m = 5.5$ (b). The values in the horizontal midplane are shown, bright areas indicating positive values.

The square pattern appears via the skewed-varicose [34] instability of primary rolls (details are described in [24]). Depending on the initial conditions, cells with rising or descending motion in the center appear. The spectrum of the excited Fourier modes shows that the asymmetric squares can be represented to lowest order by

$$\left(A_1 e^{i\mathbf{k_1 x}} + A_2 e^{i\mathbf{k_2 x}}\right) + \left(B_1 e^{i(\mathbf{k_1}+\mathbf{k_2})\mathbf{x}} + B_2 e^{i(\mathbf{k_1}-\mathbf{k_2})\mathbf{x}}\right) + c.c. \tag{15}$$

where $\mathbf{k_1}$ and $\mathbf{k_2}$ are horizontal wave numbers with $\mathbf{k_1} \perp \mathbf{k_2}$, $|\mathbf{k_1}| = |\mathbf{k_2}| = k$ being the fundamental wave number of the square pattern ($2\pi/k$ the side length of the asymmetric squares). Eq. (15) represents a superposition of two checkerboard or symmetric square patterns, one with the fundamental wave number and the other, rotated by an angle of $\pi/4$, with the wave number $q = |\mathbf{k_1} + \mathbf{k_2}| = \sqrt{2}k$, which is the wave number of the skewed varicose unstable rolls. We find the two checkerboard pattern solutions to be always unstable. However, rolls with the smaller wave number k are stable in the region where we observe stable asymmetric squares. The wave numbers k and q are in resonance through triadic interactions of the associated wave vectors. A representation like Eq. (15) was used in [28] to study square cells in non-Boussinesq convection near onset and is contained in a more general Galerkin ansatz used in [23] to study asymmetric squares in Boussinesq convection. Asymmetric squares were also found numerically in compressible magnetoconvection near onset [35].

Without rotation, the checkerboard pattern solutions are symmetric to reflections in vertical planes parallel to one of the sides of a square (additionally there is a symmetry to up-down reflections combined with horizontal translations by one square), implying zero net helicity H (since the pseudoscalar H changes sign under reflections). Furthermore, we find these solutions to be incapable of kinematic dynamo action for $T = 0$.

The bifurcation of the asymmetric squares from the rolls with wave number q being apparently subcritical [24], simulations starting from a superposition of the unstable rolls with a small perturbation lead, depending on the perturbation added to the rolls, either to asymmetric squares or to rolls of wave number k as final states. In the case of $T = 0$, the square solutions obtained may or may not possess horizontal D_4 symmetry. For the D_4 symmetric solutions one has $A_1 = A_2$ and $B_1 = B_2$ in Eq. (15). Like for the checkerboard pattern solutions, symmetry to reflections in vertical planes then implies $H = 0$. We also find the asymmetric square solutions with horizontal D_4 symmetry (obtainable only for $T = 0$) to be incapable of kinematic dynamo action.

In the following we report results for solutions lacking the horizontal D_4 symmetry at $T = 0$. For these we always find the D_4 symmetry to be completely broken. In particular, all reflection symmetries are absent, allowing a nonzero

net helicity even in the absence of rotation. Fig. 5(a) shows the helicity of a

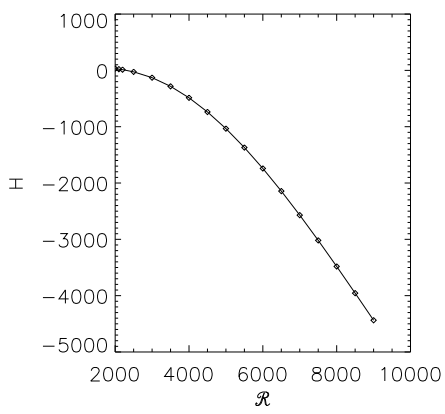

(a)

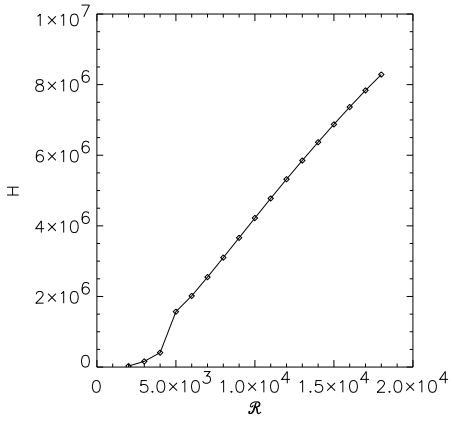

(b)

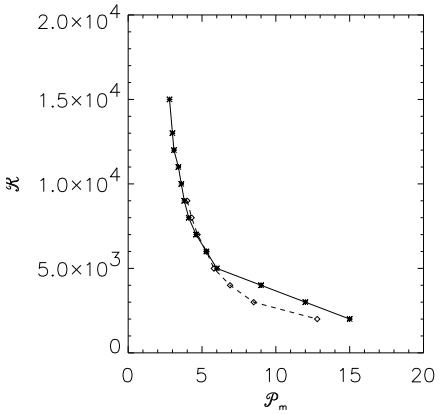

(c)

Fig. 5. The helicity of an upflow square as a function of the Rayleigh number for (a) $T = 0$ and (b) $T = 100$. The lower panel (c) shows stability boundaries for the kinematic dynamo instability in the P_m-R_a plane, the dashed line corresponding to the nonrotating case and the continuous line to $T = 100$.

nonrotating upflow square as a function of R_a in the range where the flow is stationary. Rotation at low rates about the vertical axis leaves the asymmetric squares stable. The stability boundary towards higher values of R_a, where the pattern loses stability to different kinds of oscillations, is shifted upwards compared to the case without rotation. The helicity due to rotation [see Fig. 5(b)] is much larger than the "self-helicity" of the nonrotating squares already for small T.

Through solving the magnetic induction equation the kinematic dynamo prop-

erties of the asymmetric squares were determined. In Fig. 5(c) results for $T = 0$ and $T = 100$ are given. The two curves in the P_m-R_a plane are stability boundaries where a single real eigenvalue becomes positive and the dynamo starts. An example of the generated magnetic field is depicted in Fig. 4(b). The flow stretches and folds the magnetic field lines and concentrates magnetic flux near cell boundaries.

Traditionally, it is assumed that the introduction of nonlinearity leads to a saturation of the exponential growth of the magnetic field and to a modified velocity field that maintains the magnetic field at a finite amplitude. However, recent investigations show that the back-reaction of the magnetic field can also extinguish the dynamo. This was observed for flow in triply periodic Cartesian geometry driven by an explicit forcing [36], spherical dynamo models with rotation and explicit forcing [37] and two-dimensional convection rolls in a plane layer rotating about an oblique axis [20]. Fig. 6(a) shows the time

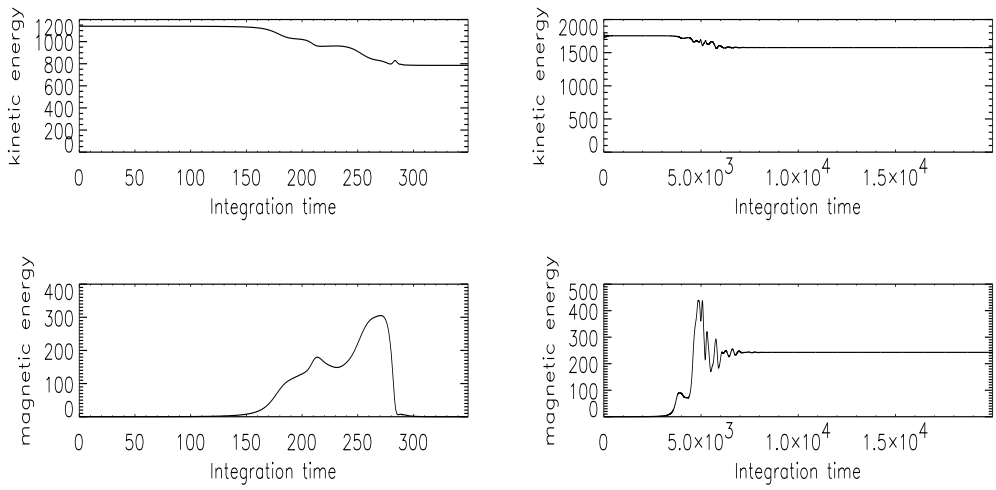

(a) (b)

Fig. 6. Time evolutions of kinetic and magnetic energies for (a) $T = 0$, $R_a = 5000$ and $P_m = 6$ and (b) $T = 10$, $R_a = 7000$ and $P_m = 4.65$.

evolutions of magnetic and kinetic energies starting from a square pattern and a small seed magnetic field for $T = 0$. Initially the magnetic field grows exponentially with a well defined growth rate. In this kinematic phase the Lorentz force is negligible and the square pattern remains undisturbed. After reaching a sufficient strength the magnetic perturbation forces the solution into the basin of attraction of the two-dimensional roll state with wave number k. The roll solution is incapable of dynamo action and the magnetic field decays to zero.

In order to achieve nonlinear dynamo action additional effects have to be in-

cluded. We consider background rotation at very low rates ($0 \leq T \leq 150$) where the asymmetric square pattern is not affected by hydrodynamical instabilities. Although the mechanism underlying the self-extinguishing is still acting, there are parameter ranges where a nonlinear dynamo is found. Time evolutions of kinetic and magnetic energies in such a case are shown in Fig. 6(b). After the initial kinematic phase, a back reaction of the magnetic field is clearly visible. But though the velocity field is modified, it still corresponds to an asymmetric square pattern. The magnetic field saturates and is maintained for all time. A necessary condition for nonlinear dynamo action is a certain balance between the Coriolis and Lorentz forces. A similar balance between these forces characterizes the strong-field branch of the Childress-Soward [19] dynamo where in a *rapidly* rotating layer the Lorentz force counteracts the Coriolis force such as to facilitate convection [32].

4 Conclusion

We have demonstrated the dynamo effect by means of two examples in which the fluid was driven by two different kinds of forcing. In one case an explicit forcing of the ABC type was used, motivated by the kinematic dynamo properties of the ABC flow. The other example was thermal convection in a plane layer.

The first bifurcation of the ABC forced system is a symmetry preserving Hopf bifurcation generating solutions with a nonvanishing magnetic field that depend periodically on time. Concentrations of the magnetic energy were found around the stagnation points of the α type, which have two-dimensional stable and one-dimensional unstable manifolds and which survive the bifurcation. The mechanism of stretching, twisting and folding, which works in their vicinity, thus continues to operate in the nonlinear regime.

By using a generalized ABC forcing the degree of helicity in the force field and thus in the generated flow could be varied. In order that the primary bifurcation leads to a dynamo, the degree of helicity in the forcing has to exceed a threshold value.

For the thermally driven system we have concentrated on the dynamo properties of asymmetric square convection. Cases without rotation and with weak rotation about a vertical axis were considered. There exist solutions with flows possessing a net kinetic helicity and being capable of kinematic dynamo action in the presence as well as in the absence of rotation. In the nonrotating case these flows are, however, always only kinematic, not nonlinear dynamos. Nonlinearly the back-reaction of the magnetic field then forces the solution into the basin of attraction of a roll pattern incapable of dynamo action. But with

rotation added parameter regions are found where the Coriolis force counteracts the Lorentz force in such a way that the self-extinguishing of the dynamo by the Lorentz force is prevented. The dynamo-generated magnetic flux tends to be concentrated near cell boundaries.

References

[1] H. K. Moffatt, Magnetic Field Generation in Electrically Conducting Fluids, Cambridge University Press, Cambridge, England, 1978.

[2] F. Krause, K.-H. Rädler, Mean-Field Magnetohydrodynamics and Dynamo Theory, Akademie-Verlag, Berlin, 1980.

[3] P. H. Roberts, A. M. Soward, Dynamo theory, Ann. Rev. Fluid Mech. 24 (1992) 459–512.

[4] V. I. Arnold, Sur la topologie des êcoulements stationnaires des fluides parfaits, C. R. Acad. Sci. Paris 261 (1965) 17–20.

[5] V. I. Arnold, E. I. Korkina, The growth of a magnetic field in a three-dimensional steady incompressible flow (in Russian), Vest. Mosk. Univ. Mat. Mekh. 3 (1983) 43–46.

[6] D. Galloway, U. Frisch, Dynamo action in a family of flows with chaotic streamlines, Geophys. Astrophys. Fluid Dyn. 36 (1986) 53–83.

[7] F. Feudel, N. Seehafer, O. Schmidtmann, Fluid helicity and dynamo bifurcations, Phys. Lett. A 202 (1995) 73–78.

[8] F. Feudel, N. Seehafer, O. Schmidtmann, Bifurcation phenomena of the magnetofluid equations, Math. Comput. Simulat. 40 (1996) 235–245.

[9] N. Seehafer, F. Feudel, O. Schmidtmann, Nonlinear dynamo with ABC forcing, Astron. Astrophys. 314 (1996) 693–699.

[10] F. Feudel, N. Seehafer, B. Galanti, S. Rüdiger, Symmetry-breaking bifurcations for the magnetohydrodynamic equations with helical forcing, Phys. Rev. E 54 (1996) 2589–2596.

[11] O. Schmidtmann, F. Feudel, N. Seehafer, Nonlinear Galerkin methods for the 3D magnetohydrodynamic equations, Int. J. Bifurcation and Chaos 7 (1997) 1497–1507.

[12] O. Schmidtmann, F. Feudel, N. Seehafer, Nonlinear Galerkin methods based on the concept of determining modes for the magnetohydrodynamic equations, J. Phys. A: Math. Gen. 31 (1998) 7141–7155.

[13] S. Rüdiger, F. Feudel, N. Seehafer, Dynamo bifurcations in an array of driven convectionlike rolls, Phys. Rev. E 57 (1998) 5533–5538.

[14] T. Dombre, U. Frisch, J. M. Greene, M. Hénon, A. Mehr, A. M. Soward, Chaotic streamlines in the ABC flows, J. Fluid Mech. 167 (1986) 353–391.

[15] B. Galanti, P. L. Sulem, A. Pouquet, Linear and non-linear dynamos associated with ABC flows, Geophys. Astrophys. Fluid Dyn. 66 (1992) 183–208.

[16] V. I. Arnold, On the evolution of a magnetic field under the influence of advection and diffusion (in Russian), in: V. M. Tikhomirov (Ed.), Some Problems of Modern Analysis, Moscow State University, 1984, pp. 8–21.

[17] D. Galloway, U. Frisch, A note on the stability of a family of space-periodic Beltrami flows, J. Fluid Mech. 180 (1987) 557–564.

[18] A. Brandenburg, R. L. Jennings, Å. Nordlund, M. Rieutord, R. F. Stein, I. Tuominen, Magnetic structures in a dynamo simulation, J. Fluid Mech. 306 (1996) 325–352.

[19] S. Childress, A. M. Soward, Convection driven hydromagnetic dynamo, Phys. Rev. Lett. 29 (1972) 837–839.

[20] P. C. Matthews, Dynamo action in simple convective flows, Proc. R. Soc. London A 455 (1999) 1829–1840.

[21] M. Assenheimer, V. Steinberg, Observation of coexisting upflow and downflow hexagons in Boussinesq Rayleigh-Bénard convection, Phys. Rev. Lett. 76 (1996) 756–759.

[22] R. M. Clever, F. H. Busse, Hexagonal convection cells under conditions of vertical symmetry, Phys. Rev. E 53 (1996) R2037–R2040.

[23] F. H. Busse, R. M. Clever, Asymmetric squares as an attracting set in Rayleigh-Bénard convection, Phys. Rev. Lett. 81 (1998) 341–344.

[24] A. Demircan, N. Seehafer, Nonlinear square patterns in Rayleigh-Bénard convection, Europhys. Lett. 53 (2001) 202–208.

[25] D. S. Oliver, J. R. Booker, Planform of convection with strongly temperature-dependent viscosity, Geophys. Astrophys. Fluid Dyn. 27 (1983) 73–85.

[26] K. Eckert, M. Bestehorn, A. Thess, Square cells in surface-tension-driven Bénard convection: experiment and theory, J. Fluid Mech. 356 (1998) 155–197.

[27] M. F. Schatz, S. J. VanHook, W. D. McCormick, J. B. Swift, and H. L. Swinney, Time-independent square patterns in surface-tension-driven Bénard convection, Phys. Fluids 11 (1999) 2577–2582.

[28] M. R. E. Proctor, P. C. Matthews, $\sqrt{2}$: 1 resonance in non-Boussinesq convection, Physica D 97 (1996) 229–241.

[29] S. Scheel, N. Seehafer, Bifurcation to oscillations in three-dimensional Rayleigh-Bénard convection, Phys. Rev. E 56 (1997) 5511–5516.

[30] A. Demircan, S. Scheel, N. Seehafer, Heteroclinic behavior in rotating Rayleigh-Bénard convection, Eur. Phys. J. B 13 (2000) 765–775.

[31] G. Küppers, D. Lortz, Transition from laminar convection to thermal turbulence in a rotating fluid layer, J. Fluid Mech. 35 (1969) 609–620.

[32] M. G. St. Pierre, The strong field branch of the Childress-Soward dynamo, in: M. R. E. Proctor, P. C. Matthews, A. M. Rucklidge (Eds.), Theory of Solar and Planetary Dynamos, Cambridge University Press, Cambridge, 1993, pp. 295–302.

[33] C. A. Jones, P. H. Roberts, Convection-driven dynamos in a rotating plane layer, J. Fluid Mech. 404 (2000) 311–343.

[34] F. H. Busse, R. M. Clever, Instabilities of convection rolls in a fluid of moderate Prandtl number, J. Fluid Mech. 91 (1979) 319–335.

[35] P. C. Matthews, M. R. E. Proctor, N. O. Weiss, Compressible magneto-convection in three dimensions: planforms and nonlinear behaviour, J. Fluid Mech. 305 (1995) 281–305.

[36] N. H. Brummell, F. Cattaneo, S. M. Tobias, Linear and nonlinear dynamo action, Phys. Lett. A 249 (1998) 437–442.

[37] H. Fuchs, K.-H. Rädler, M. Rheinhardt, On self-killing and self-creating dynamos, Astron. Nachr. 320 (1999) 129–133.